Neoplasma 2025; 72(6): 394–404

doi:10.4149/neo_2025_250422N178

Integrated transcriptomic and proteomic analysis reveals the mechanistic role of OST in cutaneous squamous cell carcinoma

Yue WANG[1,#], Hongfang DING[2,#], Tong GAO[1], Bocheng JI[1], Yan GAO[3], Wenjie YAN[1,*], JUANWANG[2,3,*]

[1]Department of Dermatology, The Affiliated Hospital of Guilin Medical University, Guilin, China; [2]Faculty of Basic Medicine, Guilin Medical University, Guilin, China; [3]Nurse of College, Guilin Medical University, Guilin, China

**Correspondence: ywj716@glmc.edu.cn; juanlovelife@163.com*
#Contributed equally to this work.

Received April 22, 2025 / Accepted November 24, 2025

Osthole (OST) is a natural component of the traditional Chinese medicinal herb, *Cnidium monnieri*, that exhibits antipruritic properties and may exert effects on dermatitis. Numerous previous studies have focused on the effects of OST in tumors; however, the potential impact on cutaneous squamous cell carcinoma (CSCC) remains to be fully elucidated. Thus, the present study aimed to evaluate CSCC cell proliferation following treatment with OST, and further analyzed the underlying mechanisms using multi-omics analyses. Due to their cancerous characteristics, both A431 and SCL-1 cells are used in drug screening and testing for CSCC, particularly for therapies targeting growth pathways and markers associated with SCC. Results of the flow cytometry analysis demonstrated that OST impacted the CSCC cell cycle, causing arrest in the G2 phase. Notably, OST exerted a slight growth-promoting effect on healthy skin HaCaT cells. In addition, our omics results revealed that there were 1,720 differentially expressed genes and 227 differentially expressed proteins in the OST-treated group. Transcriptomics combined with proteomics analyses revealed that 5 of the top 20 screened pathways were associated with the cell cycle, and ATR, CENPJ, and RAD54B were highlighted as specific targets for OST-mediated regulation. Collectively, these results suggested that OST has a potential inhibition on human CSCC cells, and ATR, CENPJ, and RAD54B may be the key factors regulated by OST in A431's cell cycle progression inhibition.

Key words: transcriptomics; proteomics; cell cycle arrest; OST; cutaneous squamous cell carcinoma

Cutaneous squamous cell carcinoma (CSCC) is characterized by the malignant proliferation of keratin-forming cells derived from the epidermis and its appendages, including hair follicles, sebaceous glands and small sweat glands [1, 2]. Ranking as the second most prevalent skin malignancy in humans, CSCC constitutes ~33% of all non-melanoma skin cancers [2, 3]. The notable rates of occurrence and mortality place substantial physical, psychological, and economic burdens on affected individuals. At present, surgery is the primary treatment option for CSCC, with radiation therapy, chemotherapy, and laser treatment used as secondary or adjuvant treatments [4, 5]. However, CSCC primarily affects individuals between 50 and 70 years of age, who are often at an increased risk of surgical complications, and may present with a lower tolerance to potential side effects associated with radiation and chemotherapy [6]. Therefore, further investigations are necessary to develop novel treatment options that demonstrate high levels of efficacy and safety.

Osthole (OST) is a traditional Chinese medicine that exhibits antipruritic properties and exerts potential effects on dermatitis. Thus, the present study aimed to determine the potential impact of OST on CSCC. Notably, natural medicines may play an important role in the treatment of cancer [7]. OST is a coumarin compound extracted from the fruit of the traditional Chinese medicinal herb, *Cnidium monnieri* [8]. The chemical structure of OST is 7-methoxy-8-isopentenyl-coumarin with a molecular weight of 244.29 [9]. Results of previous studies demonstrated that OST is associated with minimal toxic side effects, a broad safety profile, affordability, and high levels of tolerability in humans. In addition, OST exhibits a wide range of pharmacological activities, including anti-cancer, anti-inflammatory, antioxidant, and antipruritic properties [9, 10]. Previous studies have demonstrated the inhibitory effects of OST on the growth of malignant tumors, including breast cancer, ovarian cancer, colorectal cancer, lung cancer, and hepatocellular carcinoma [11–18].

In this study, we found that OST inhibited the proliferation of CSCC cells (A431 and SLC-1 cell lines). Moreover, it exerted minimal inhibitory effects on the healthy skin HaCaT cell line, indicating the potential for this drug in the treatment of CSCC. Small-molecule drugs, including bioactive natural drugs, exert their desired pharmacological functions through interactions with specific targets. However, the potential targets and mechanisms of OST in CSCC remain to be fully elucidated.

Given that small-molecule drugs exert their pharmacological effects through interactions with specific targets, identifying these targets is essential for validating the mechanism of OST action [19]. In this study, we aimed to determine the potential targets and mechanisms of OST in the treatment of CSCC, through phenotype-based screening combined with integrated transcriptomic and proteomic analyses [20, 21].

Materials and methods

Cell lines. Human epidermal cancer cell lines, namely, A-431 cells, were purchased from Pricella Company, SCL-1 cells were obtained from Otwo Biotech Company (Catalog No. HTX2657), and HaCaT cells from Ubigene Company. We validated the origin of HaCaT cells using STR analysis.

Reagents and antibodies. OST was purchased from Push Biotechnology Co., Ltd. (purity ≥ 99%, Chengdu, China). Dulbecco's Modified Eagle's Medium (DMEM) and FBS were obtained from Gibco; Thermo Fisher Scientific, Inc. MTT and penicillin-streptomycin were purchased from Beijing Solarbio Science & Technology Co., Ltd. The BCA assay kit, phenylmethylsulphonyl fluoride (PMSF), and radioimmunoprecipitation assay (RIPA) were purchased from Beyotime Institute of Biotechnology. Anti-CENPJ (#TA811852S) was purchased from OriGene Technologies, Inc., and anti-ATR (#P11588) and anti-RAD54B (#P33254) were obtained from Promab Biotechnologies, Inc.

Cell culture. A431, HaCaT, and SCL-1 cells were cultured in DMEM supplemented with 10% FBS and 1% penicillin-streptomycin to support their growth and proliferation. All cell lines were kept in a humidified incubator at 37°C with 5% CO_2.

Cell viability assay. OST was dissolved in DMSO at a concentration of 640 mmol/l, and SCL-1 and A431 cells were seeded into 96-well plates. On day 2, OST was diluted with cell culture medium to reach final concentrations of 40, 80, 160, and 320 μmol/l. Seeded cells were treated with differing concentrations of diluted OST for 24, 48, and 72 h. Subsequently, MTT was added, and cells were incubated for 4 h at 37°C. Following the addition of 150 μl of DMSO, cell viability was determined at a wavelength of 490 nm using a microplate reader (Tecan Group, Ltd.).

Colony formation assay. Following trypsin digestion, A431 cells were harvested via centrifugation and seeded uniformly at a density of 100 cells/well in a 6-well plate. On day 2, OST was added to wells at varying concentrations (0, 160, and 320 μmol/l), and culture medium was replaced every 3 days. Following 12 days of treatment with OST, cells were fixed using 4% paraformaldehyde and stained with 0.1% crystal violet. Subsequently, cells were washed 3 times with PBS, and plates were air-dried and scanned using a chemiluminescence imaging system. The inhibition rate of clone formation was calculated using the following formula: Inhibition rate (%) = [(Number of colonies in the control group – Number of colonies in the treatment group)/Number of colonies in the control group] × 100.

Flow cytometry. Following treatment with OST (320 μmol/l) for 48 h, A431 cells were digested with 0.25% trypsin, harvested by centrifugation, and finally washed twice with ice-cold PBS. Subsequently, cells were immobilized using 70% ice-cold ethanol and incubated overnight at –20°C. Following incubation, cells were collected via centrifugation and washed twice with ice-cold PBS. Cells were subsequently incubated with RNase for 30 min and stained with propidium iodide (50 μg/ml) in the dark. After 30 min, cell cycle analysis was performed using flow cytometry (Accuri™C6 Plus Flow Cytometer, Becton Dickinson, San Jose, CA, USA) and Flowjo software (Flowjo™10, Becton Dickinson, San Jose, CA, USA).

RNA sequencing (RNA-seq) analysis. A431 cells were treated with 160 μmol/l OST for 48 h and harvested for RNA-seq analysis, as described previously [22]. The RNA-seq data for this study have been submitted to the NCBI Sequence Read Archive (SRA) under BioProject accession number PRJNA1218291 (Temporary Submission ID: SUB15056061). SRA records will be accessible with the following link after the indicated release date: https://www.ncbi.nlm.nih.gov/sra/PRJNA1218291

Proteomics analysis. A431 cells were treated with 160 μmol/l OST for 48 h and harvested for proteomics analysis, as described previously [22]. The proteomics data have been submitted to the ProteomeXchange Consortium with the accession number PXD060279.

Western blot analysis. A431 cells were treated with OST for 48 h. Total protein was extracted from cells using RIPA buffer supplemented with PMSF at a volume ratio of 100:1. The mixture was kept on ice to ensure protein stability during lysis. Proteins were isolated from cell lysates using centrifugation and separated via SDS-PAGE. Separated proteins were transferred onto a nitrocellulose membrane and blocked with 5% skimmed milk for 2 h. Following blocking, membranes were washed with PBS+0.05% Tween 20 and incubated with primary and secondary antibodies. Protein bands were visualized using an ECL kit, and protein expression was quantified using Image Lab software (Bio-Rad Laboratories, Inc.).

Statistical analysis. Data are presented as the mean ± standard deviation (SD), and GraphPad Prism 8 (GraphPad; Dotmatics) was used for statistical analysis. Differences between two groups were analyzed using a two-tailed Student's t-test, and differences between multiple groups

were analyzed using one-way ANOVA. A p-value <0.05 was considered to indicate a statistically significant difference.

Results

OST inhibits CSCC cell proliferation. MTT analysis demonstrated that treatment with OST inhibited the proliferation of CSCC cells in a time- and dose-dependent manner. Notably, A431 cells exhibited a higher sensitivity to OST. Compared with the control group, cells appeared brighter with an abnormal morphology following treatment with OST (Figure 1A). As displayed in Figures 1B and 1C, OST significantly inhibited the proliferation of A431 and SLC-1 CSCC cell lines. Compared with the control group, ~90% of cell proliferation was inhibited by 320 μmol/l OST. In addition, to detect the cell toxicity of OST on normal human healthy skin

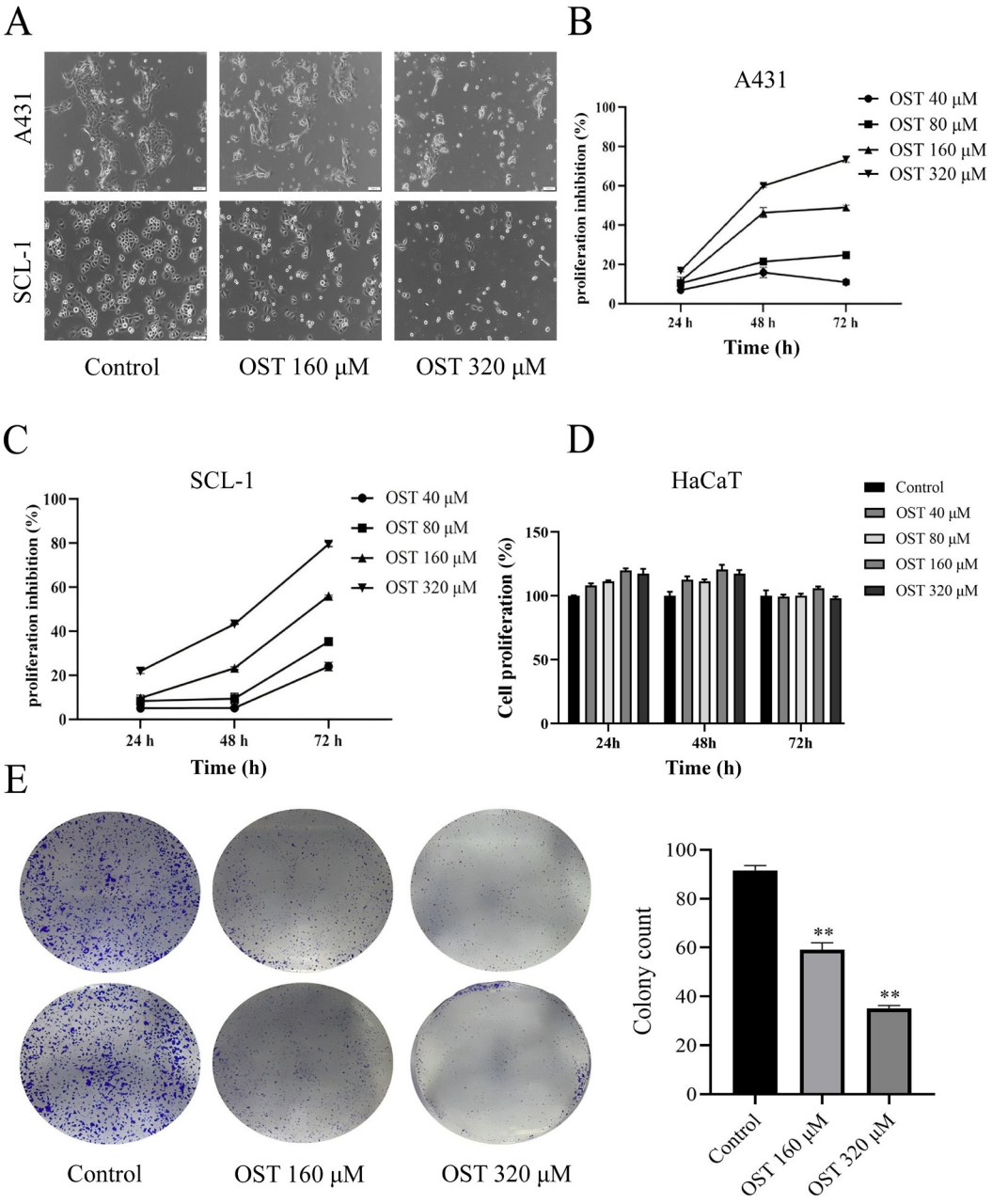

Figure 1. OST inhibited cutaneous squamous cell carcinoma cells' proliferation. A) Microscopic morphological changes in skin squamous cell carcinoma cells induced by OST. B–D) The proliferation inhibition effect of OST on A431, SCL-1, and HaCaT cell lines. E) Colony formation assays were used to analyze A431 cells with and without OST treatment (0, 160, and 320 μmol/l). Data are expressed as the mean ± SD from three independent experiments. **p<0.05 compared with the control group

cells, we analyzed the cell growth of HaCaT cells after treatment with OST, and the results showed that there was a slight growth-promoting effect of OST (Figure 1D). The colony formation assay showed that OST exerted inhibitory effects on the proliferation of CSCC cells (Figure 1E). Collectively, these results indicated that OST may exert antiproliferative effects on CSCC cells, with low levels of cytotoxicity in the healthy skin HaCaT cell line.

OST induces cell cycle arrest in CSCC cells. Uncontrolled and rapid cell division is a hallmark of cancer cells. Notably, numerous natural drugs exert inhibitory effects on cancer cells by inhibiting cell cycle progression. Thus, the present study aimed to determine the effects of OST on cell cycle arrest in CSCC cells. A431 cells treated with or without 320 μmol/l OST were analyzed via flow cytometry. As displayed in Figures 2A and 2B, the cell cycle of A431 cells treated with OST was arrested at the S phase. Furthermore, we measured DNA synthesis using EdU staining assays and found that OST significantly inhibited DNA synthesis in SCL-1 cells (Supplementary Figure S1). The absence of a sub-G1 population in the data is due to the gating strategy employed during flow cytometry analysis. Specifically, the gating excluded dead cells, which were not included in the analysis. As a result, the sub-G1 population, which typically represents apoptotic cells, was not detected. This explains the discrepancy and aligns with the description of OST-induced cell death.

RNA-seq analysis of differentially expressed genes following treatment with OST. In the present study, RNA-seq analysis was used to determine potential transcrip-

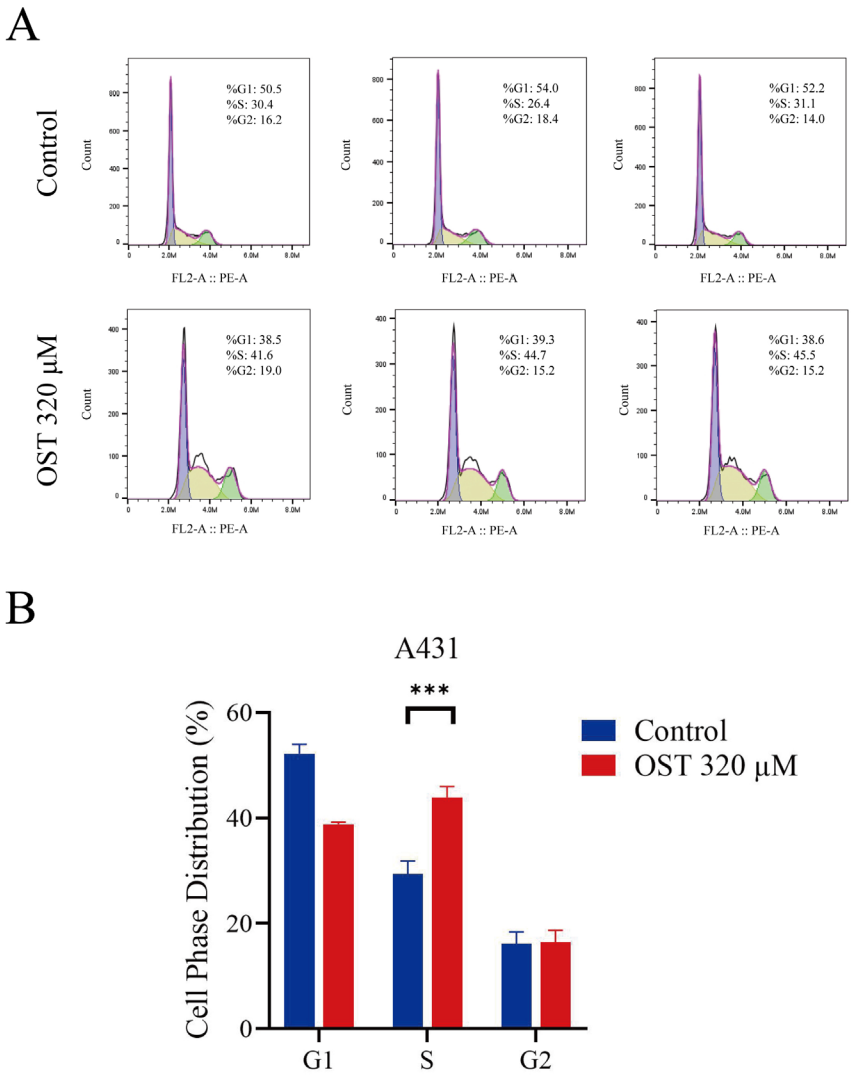

Figure 2. OST induced cutaneous squamous cell carcinoma cell cycle arrest. A) Representative flow cytometry images of the A431 cells treated or untreated with OST are shown. B) The percentage of cells in different phases of the cell cycle is represented as a bar diagram. *p<0.05, ***p<0.001 compared with the control group. Three independent experiments were performed to validate the findings.

tomic alterations in A431 cells following treatment with OST. Principal component analysis (PCA) revealed significant variations in RNA abundance between OST-treated cells and those in the control group (Figure 3A). Heatmap and volcano plots were used to illustrate the transcripts exhibiting differential expression (Figures 3B, 3C). In the present study, a total of 20,036 RNAs were quantified, with 1,720 RNAs exhibiting statistically significant alterations following OST

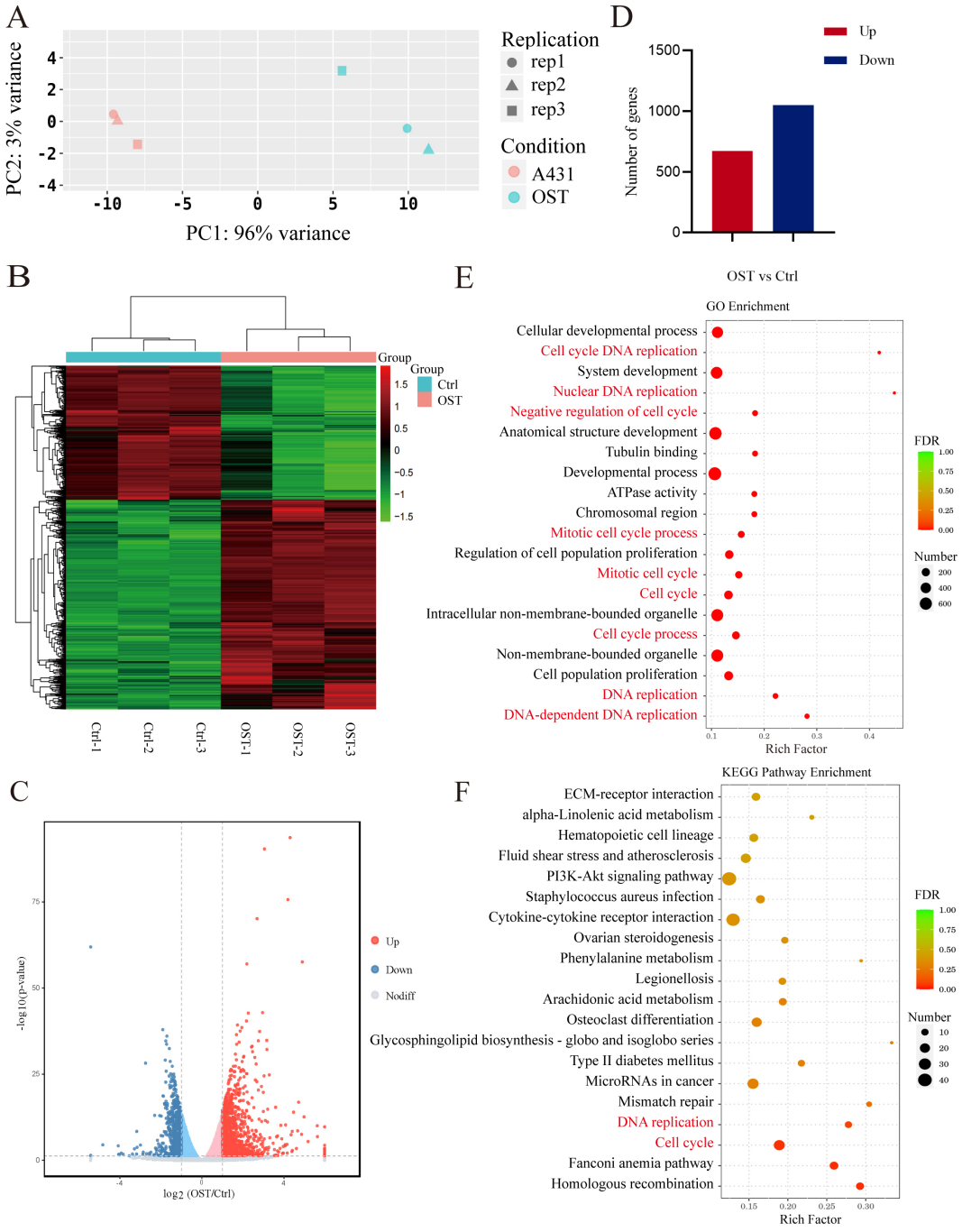

Figure 3. Differential analysis of gene expression levels between control and OST-treated A431 cells. A) Principal component analysis was applied to the RNA-seq data, with each point on the plot representing a biological replicate. B) Heatmap illustrating gene expression differences among various groups. C) Volcano plots depicting the transcript abundance variations, with gray dots indicating no statistically significant differences. Significantly upregulated proteins are represented by red dots, while significantly downregulated proteins are denoted by blue dots. D) Histogram depicting the variation in gene expression across different groups; E, F) Both of them annotations for GO and KEGG terms were performed for genes.

treatment. Among these, the expression levels of 1,048 genes were reduced, while the expression levels of 672 genes were increased (Figure 3D). Differentially expressed gene functions were annotated using the Kyoto Encyclopedia of Genes and Genomes (KEGG) and Gene Ontology (GO) databases. Results of the GO enrichment analysis demonstrated that the differentially expressed genes altered following treatment with OST were enriched in pathways closely associated with the cell cycle, such as cell cycle progression, DNA replication, negative regulation of the cell cycle, and the mitotic cell cycle process (Figure 3E). Notably, these pathways accounted for nine of the top 20 pathways. KEGG enrichment analysis revealed that the pathways altered following treatment with OST were enriched in biological regulatory processes, including DNA replication, cell cycle, PI3K-AKT signaling pathways, and cytokine-cytokine receptor interaction (Figure 3F). Collectively, these results highlighted that OST may exert effects in CSCC through inhibition of cell cycle progression.

Proteomics analysis of differentially expressed proteins following treatment with OST. Subsequently, data-independent acquisition (DIA) protein-quantification proteomics analysis was used to identify specific proteins that were impacted following treatment with OST. In the present study, a total of 7,628 proteins were identified through DIA quantitative proteomics analysis. PCA analysis revealed significant variations in protein abundance between OST-treated cells and those in the control group (Figure 4A). Heat maps and volcano plots were used to illustrate the proteins exhibiting differential expression (Figures 4B, 4C). Differential protein expression levels in OST-treated and control groups are displayed in Figure 3C. Out of 7,628 identified proteins, 282 proteins were significantly altered following OST treatment, with downregulation of 55 proteins and upregulation of 227 proteins (Figure 4D). Results of the GO enrichment analysis revealed that the differentially expressed proteins altered following treatment with OST were enriched in biological processes associated with the regulation of mitochondria, ribosomes, oxidative phosphorylation, DNA replication, and the cell cycle. Among the top 20 enrichment pathways, two pathways were associated with the cell cycle (Figure 4E). Moreover, results of the KEGG enrichment analysis revealed that the differentially expressed proteins altered by OST were involved in oxidative phosphorylation, DNA replication, and the cell cycle (Figure 4F).

Potential association between the transcriptome and proteome. To determine the potential association between the gene and protein expression alterations observed following treatment with OST, an integrated analysis of transcriptomics and proteomics was carried out. Venn analysis revealed 69 overlapping molecules that exhibited significant differential expression at both gene and protein levels (Figure 5A). Among them, 60 molecules exhibited consistent expression trends, with 26 molecules demonstrating upregulation and 34 molecules demonstrating downregulation. However, mRNA and protein expression of the remaining nine molecules appeared to be inconsistent. Subsequently, overlapping molecules were displayed in a nine-quadrant graph. Red points were indicative of significant upregulation at both mRNA and protein levels, while green points represented overlapping downregulated genes (Figure 5B). To screen for commonly regulated pathways at both mRNA and protein levels, GO enrichment analysis was performed. Results of the present study revealed that the commonly regulated molecules were mainly enriched in the cell cycle process, and 5 of the top 20 biological processes were associated with the cell cycle (Figure 5C). Collectively, these results highlighted that pathways associated with the cell cycle may play a crucial role in mediating the anti-cancer effects of OST on CSCC cells. Subsequently, screening was carried out to identify specific molecules involved in the aforementioned cell cycle pathways that were altered following treatment with OST. The screening analysis highlighted several molecules associated with cell cycle pathways, including ATR, CENPJ, and RAD54B (Figure 5D).

***In vitro* verification of OST targets.** RNA-seq analysis results revealed that three genes exhibited a 2.55- to 3.00-fold reduced expression in OST-treated cells (Figure 6A). In addition, DIA analysis results demonstrated that the aforementioned proteins, namely, ATR, CENPJ, and RAD54B, exhibited a 2.23- to 14.03-fold reduced expression in OST-treated cells (Figure 6B). Our qPCR results (Supplementary Figure S2) and western blot analysis revealed that ATR, CENPJ, and RAD54B expression levels were reduced in A431 cells following treatment with OST (Figure 6C). Notably, these results were comparable with those obtained using proteomics analysis. Collectively, the present study revealed that these proteins may act as targets of OST for the promotion of cell cycle arrest of A431 cells.

Discussion

In recent years, research has focused on the use of traditional Chinese medicines in the treatment of cancer [7, 23]. OST is an active compound extracted from the herbal medicine, *Cnidium monnieri*. Numerous studies reported that OST may exhibit potential in inhibiting inflammation and may exhibit antitumor properties [8, 24]. Previous studies revealed that OST may exert anti-cancer activity in nasopharyngeal, gastric, ovarian, and colon cancer [13, 14, 25, 26]. Moreover, our previous studies demonstrated that OST induced necroptosis in glioma cells [27] and caused apoptosis and pyroptosis in cervical cancer cells [28]. However, further investigations are required to determine the specific anti-cancer properties of OST.

Multi-omics analysis serves as a valuable tool in the target identification stage of drug development, playing a crucial role in drug screening and the treatment of various diseases [29]. Multi-omics may provide key information about genes and proteins, revealing specific regulatory relationships and

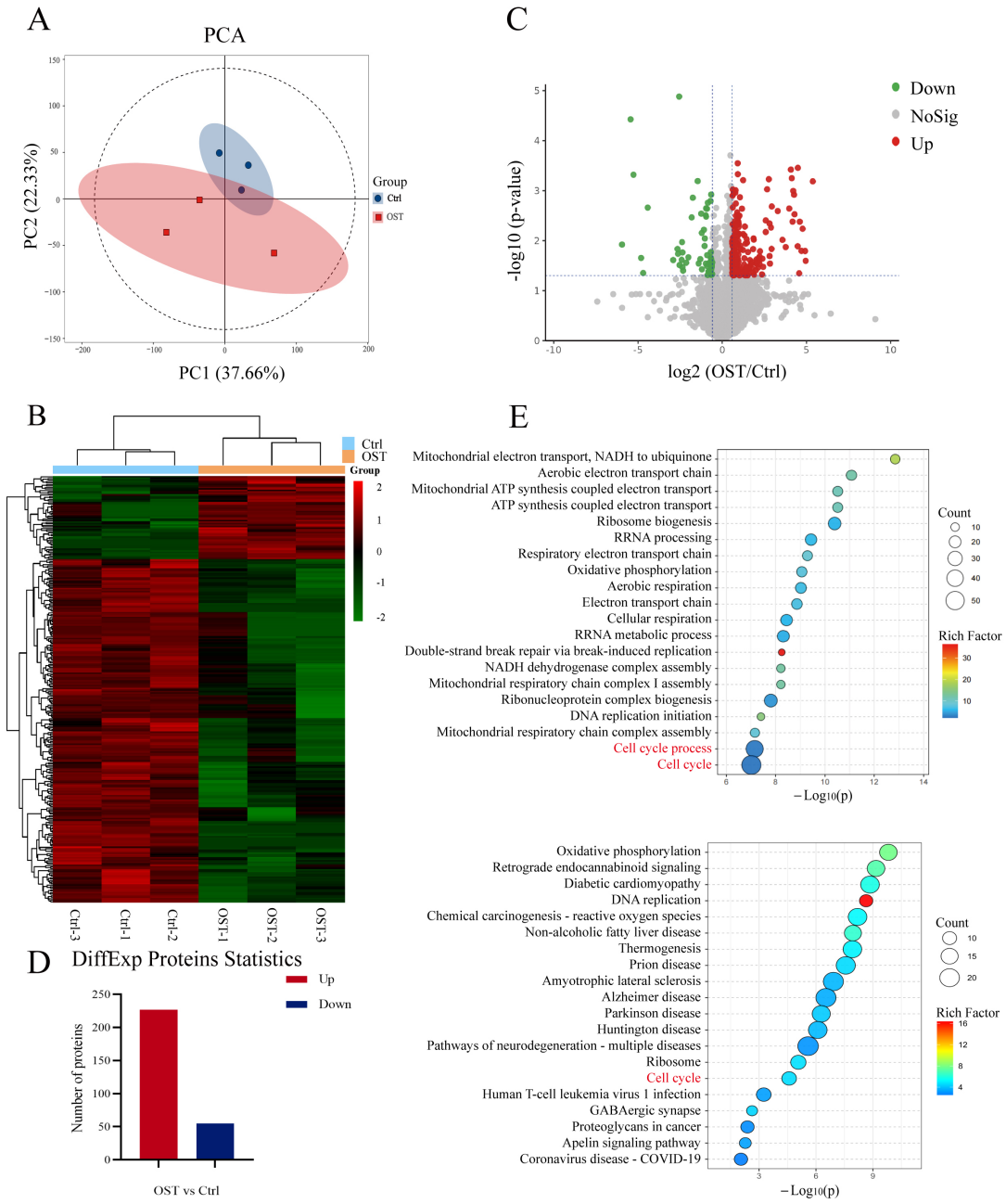

Figure 4. Differential analysis of protein expression levels between control and OST-treated A431 cells. A) Principal Component Analysis of proteomic data comparing the control and OST-treated groups. Each point on the plot represents a biological replicate. B) Heatmap illustrating the differential expression of proteins across various groups. C) The protein volcano plot depicts the abundance distribution, with gray dots indicating no statistically significant differences. Significantly upregulated proteins are represented by red dots, while significantly downregulated proteins are denoted by blue dots. D) Histogram depicting the variation in protein expression across different groups. E, F) Both of them annotations for GO and KEGG terms were performed for proteins.

interactions; thus, leading to a more comprehensive understanding of biological processes. Moreover, multi-omics aids researchers in gaining a more comprehensive understanding of the molecular mechanisms underlying diseases, uncovering potential biological processes and key signaling pathways [30, 31]. Transcriptomic and proteomic analyses utilize high-throughput sequencing technologies to study all transcribed RNA molecules and proteins in an organism [32, 33]. Transcriptomic analyses revealed that the OST-mediated inhibition of CSCC cells was associated with the cell cycle. The

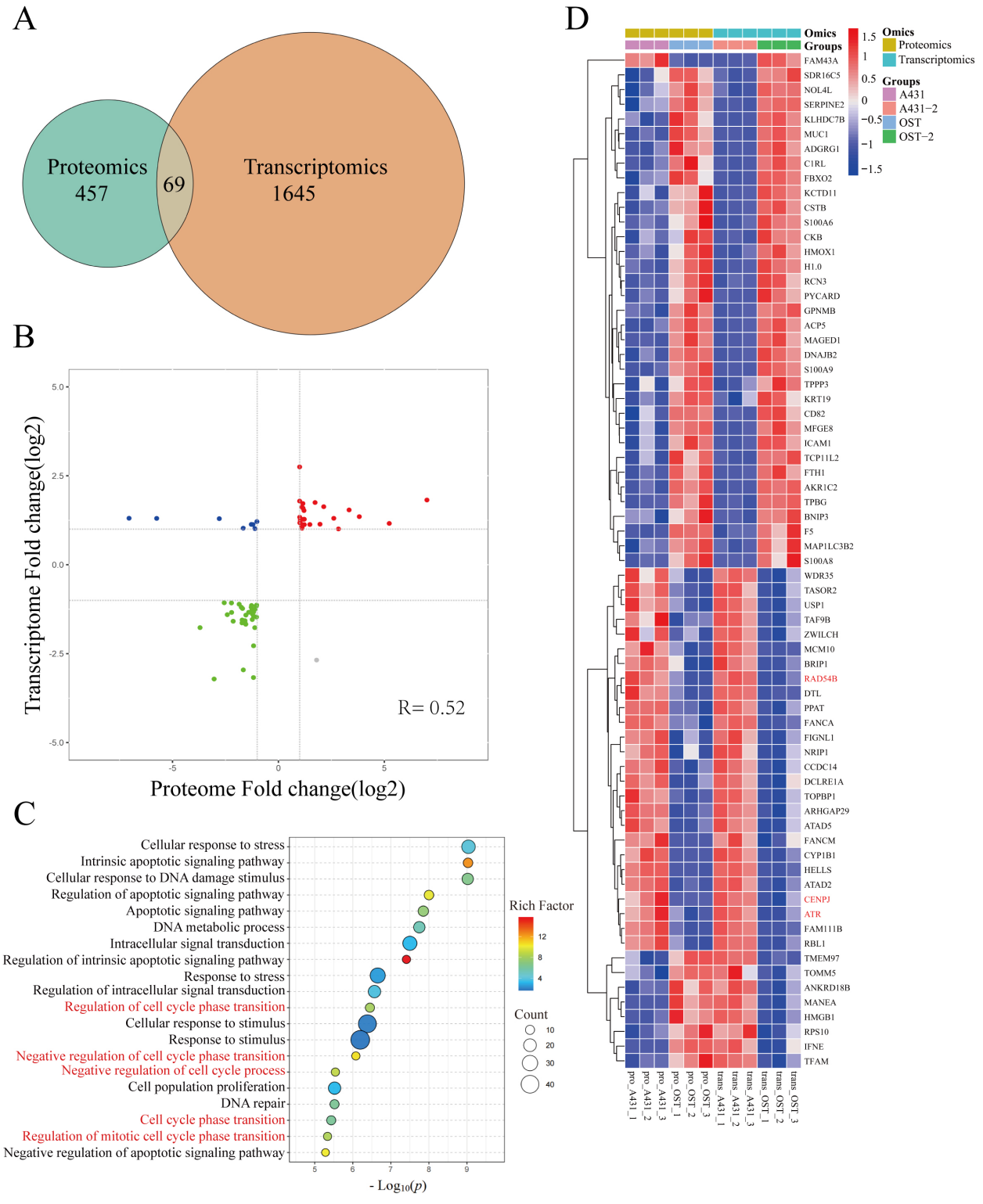

Figure 5. The relationship between the transcriptome and proteome. A) The comprehensive approach to pinpointing the pivotal targets of OST-treated A431. B) Control vs OST nine-quadrant graph. The abscissa is the fold change of the protein, the ordinate is the fold change of the transcriptome, the top of the figure is the Pearson correlation and p-value associated with the transcriptome and the proteome. Each dot represents a gene/protein. C) Annotations for GO terms were performed for overlapped downregulated molecules by OST in A431 cells. D) This heatmap illustrates the differential expression of genes across various samples categorized into different omics groups (proteomics and transcriptomics) and subgroups (A431, OST). The color scale represents relative expression levels, with red indicating upregulation and blue indicating downregulation.

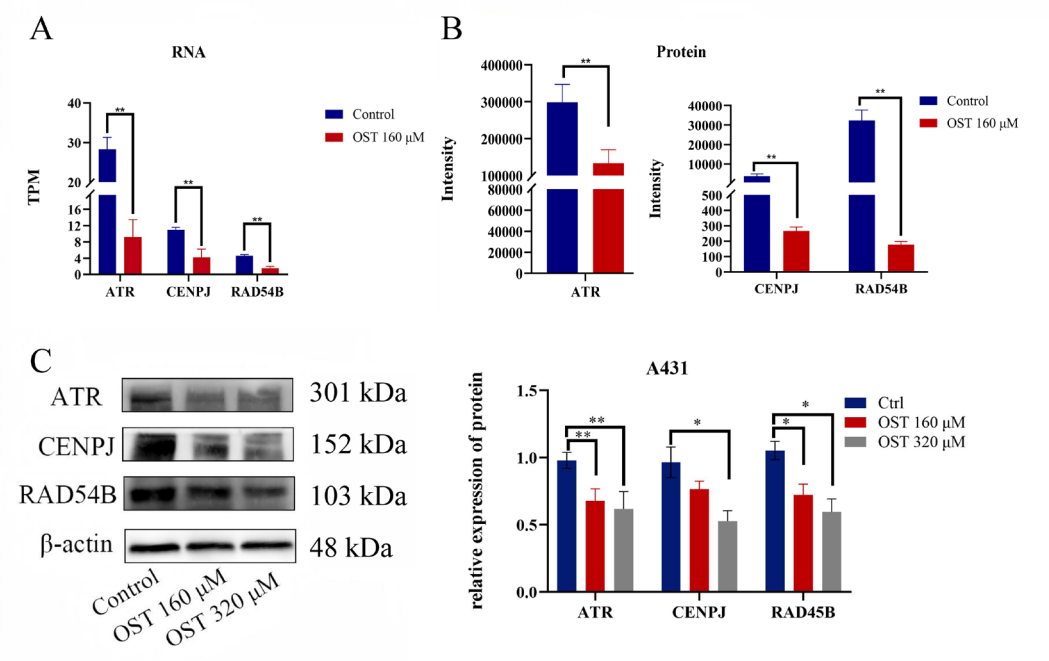

Figure 6. Differential expression of RNAs and proteins identified in A431 cells treated with OST. A) Bar charts show the enriched transcripts identified by RNA-seq for the cell cycle pathway. B) Bar charts show the enriched proteins identified by DIA for the cell cycle pathway. C) Protein expression of the indicated targets determined by western blotting assay (left) and its quantitative analysis (right). The above values are expressed as mean ± SD, n=3. *p<0.05, **p<0.01 compared with the control group.

proteomics analysis identified 288 differentially expressed proteins, and GO enrichment analysis demonstrated that 2 key pathways associated with the cell cycle were altered in A431 cells following treatment with OST. Additional proliferation assays are required to determine the effects of OST on healthy skin cells and to further understand the broader therapeutic potential of OST.

Transcriptomic and proteomic integration methods aid in identifying novel therapeutic targets for the treatment of various diseases, and highlight molecules that exhibit alterations at both gene and protein levels. This integration may lead to the development of novel drugs and treatment strategies [34]. Results of the present study revealed that overlapping genes and proteins were mainly concentrated in pathways associated with response to stimuli, apoptosis, and the cell cycle. In addition, results of the cell cycle analysis revealed that treatment with OST led to CSCC cell cycle arrest at the S phase, and these results are comparable with those obtained in previous studies [15, 35, 36]. In the present study, the proteins of ATR, CENPJ, and RAD54B associated with cell cycle progression, which were identified as key targets of OST.

ATR, a cell cycle checkpoint protein, prevents damaged or incompletely replicated DNA from entering mitosis, and inhibition of this protein may induce cell cycle arrest at the S phase [37, 38]. CENPJ, also known as CPAP, is essential for centriole duplication, and inhibition of this protein may induce multiple mitotic abnormalities [39]. RAD54B, a member of the SNF2/SWI2 superfamily, is a novel DNA damage-responsive protein that protects cells from DNA damage [40]. RAD54B regulates cell cycle progression after DNA damage and participates in homologous recombinational repair [41]. A previous study revealed that RAD54B knockout caused cells to arrest at the S phase and increased apoptosis [42]. Notably, results of the present study revealed that the protein expression levels of ATR, CENPJ, and RAD54B were reduced following treatment with OST in CSCC cells. However, further investigations are required to determine the specific molecular mechanisms associated with OST-mediated protein inhibition.

The present study focused on identifying the transcriptional regulatory mechanisms of OST. Thus, further investigations into the potential post-transcriptional modifications of OST are required, including phosphorylation, SUMOylation, and ubiquitination. In future studies, we plan to explore how overexpressing ATR, CENPJ, and RAD54B affects OST resistance. By overexpressing one of these proteins in cells, we can see if it helps cells resist OST and how it impacts the other two proteins. This will help us understand if there are compensatory or synergistic interactions between these molecules. Ultimately, our findings could provide insights into new strategies to overcome OST resistance. Moreover, further investigations are required to determine the impact of OST on cell proliferation and migration *in vitro*, and additional

in vivo experiments are required to determine the impact of OST on tumor formation.

In conclusion, the present study utilized transcriptomics and proteomics to comprehensively elucidate the mechanisms underlying OST treatment in CSCC cells. Results of the present study revealed that OST effectively inhibited the proliferation of CSCC cells and induced cell cycle arrest. In addition, the present study identified and validated 3 potential targets of OST, namely, ATR, CENPJ, and RAD54B, and these proteins were associated with cell cycle progression. Thus, the present study highlighted that ATR, CENPJ, and RAD54B may exhibit potential as therapeutic targets for the treatment of CSCC.

Supplementary information is available in the online version of the paper.

Acknowledgments: This work was supported by Guangxi Science and Technology Major Project (Guike AA23023035-7), the Guangxi Science and Technology Base and Talents Special Project (AD20238024), the Special Fund of the Central Government Guiding Local Scientific and Technological Development by Guangxi Science and Technology Department (GuikeZY21195024), the National Natural Science Foundation of China (82160768 and 82002822), and the Science and Technology Planned Project in Guilin (20210102-1).

References

[1] QUE SKT, ZWALD FO, SCHMULTS CD. Cutaneous squamous cell carcinoma: Incidence, risk factors, diagnosis, and staging. J Am Acad Dermatol 2018; 78: 237–247. https://doi.org/10.1016/j.jaad.2017.08.059

[2] CHANG MS, AZIN M, DEMEHRI S. Cutaneous Squamous Cell Carcinoma: The Frontier of Cancer Immunoprevention. Annu Rev Pathol 2022; 17: 101–119. https://doi.org/10.1146/annurev-pathol-042320-120056

[3] WALDMAN A, SCHMULTS C. Cutaneous Squamous Cell Carcinoma. Hematol Oncol Clin North Am 2019; 33: 1–12. https://doi.org/10.1016/j.hoc.2018.08.001

[4] WORK G, INVITED R, KIM JYS, KOZLOW JH, MITTAL B et al. Guidelines of care for the management of cutaneous squamous cell carcinoma. J Am Acad Dermatol 2018; 78: 560–578. https://doi.org/10.1016/j.jaad.2017.10.007

[5] GARCOVICH S, COLLOCA G, SOLLENA P, ANDREA B, BALDUCCI L et al. Skin Cancer Epidemics in the Elderly as An Emerging Issue in Geriatric Oncology. Aging Dis 2017; 8: 643–661. https://doi.org/10.14336/AD.2017.0503

[6] MAEDA T, YOSHINO K. Management of elderly patients with advanced cutaneous squamous cell carcinoma. Jpn J Clin Oncol 2022; 52: 214–220. https://doi.org/10.1093/jjco/hyab213

[7] NAEEM A, HU P, YANG M, ZHANG J, LIU Y et al. Natural Products as Anticancer Agents: Current Status and Future Perspectives. Molecules 2022; 27: 8367. https://doi.org/10.3390/molecules27238367

[8] SUN M, SUN M, ZHANG J. Osthole: an overview of its sources, biological activities, and modification development. Med Chem Res 2021; 30: 1767–1794. https://doi.org/10.1007/s00044-021-02775-w

[9] YANG S, DAI W, WANG J, ZHANG X, ZHENG Y et al. Osthole: An up-to-date review of its anticancer potential and mechanisms of action. Front Pharmacol 2022; 13: 945627. https://doi.org/10.3389/fphar.2022.945627

[10] HASSANEIN EHM, SAYED AM, HUSSEIN OE, MAHMOUD AM. Coumarins as Modulators of the Keap1/Nrf2/ARE Signaling Pathway. Oxid Med Cell Longev 2020; 2020: 1675957. https://doi.org/10.1155/2020/1675957

[11] CHEN YQ, SONG HY, ZHOU ZY, MA J, LUO ZY et al. Osthole inhibits the migration and invasion of highly metastatic breast cancer cells by suppressing ITGα3/ITGβ5 signaling. Acta Pharmacol Sin 2022; 43: 1544–1555. https://doi.org/10.1038/s41401-021-00757-7

[12] LI X, ZHANG C, WU E, HAN L, DENG X et al. UPLC-Q-TOF/MS-Based Metabolomics Approach Reveals Osthole Intervention in Breast Cancer 4T1 Cells. Int J Mol Sci 2023; 24: 1168. https://doi.org/10.3390/ijms24021168

[13] BAE H, LEE JY, SONG J, SONG G, LIM W. Osthole interacts with an ER-mitochondria axis and facilitates tumor suppression in ovarian cancer. J Cell Physiol 2021; 236: 1025–1042. https://doi.org/10.1002/jcp.29913

[14] PENG KY, CHOU TC. Osthole Exerts Inhibitory Effects on Hypoxic Colon Cancer Cells via EIF2 Phosphorylation-mediated Apoptosis and Regulation of HIF-1. Am J Chin Med 2022; 50: 621–637. https://doi.org/10.1142/S0192415X22500240

[15] XU X, ZHANG Y, QU D, JIANG T, LI S. Osthole induces G2/M arrest and apoptosis in lung cancer A549 cells by modulating PI3K/Akt pathway. J Exp Clin Cancer Res 2011; 30: 33. https://doi.org/10.1186/1756-9966-30-33

[16] YIN S, LIU H, WANG J, FENG S, CHEN Y et al. Osthole Induces Apoptosis and Inhibits Proliferation, Invasion, and Migration of Human Cervical Carcinoma HeLa Cells. Evid Based Complement Alternat Med 2021; 2021: 8885093. https://doi.org/10.1155/2021/8885093

[17] LIN ZK, LIU J, JIANG GQ, TAN G, GONG P et al. Osthole inhibits the tumorigenesis of hepatocellular carcinoma cells. Oncol Rep 2017; 37: 1611–1618. https://doi.org/10.3892/or.2017.5403

[18] MO Y, WU Y, LI X, RAO H, TIAN X et al. Osthole delays hepatocarcinogenesis in mice by suppressing AKT/FASN axis and ERK phosphorylation. Eur J Pharmacol 2020; 867: 172788. https://doi.org/10.1016/j.ejphar.2019.172788

[19] LEE H, LEE JW. Target identification for biologically active small molecules using chemical biology approaches. Arch Pharm Res 2016; 39: 1193–1201. https://doi.org/10.1007/s12272-016-0791-z

[20] JUNG HJ, KWON HJ. Target deconvolution of bioactive small molecules: the heart of chemical biology and drug discovery. Arch Pharm Res 2015; 38: 1627–1641. https://doi.org/10.1007/s12272-015-0618-3

[21] BLAY V, TOLANI B, HO SP, ARKIN MR. High-Throughput Screening: today's biochemical and cell-based approaches. Drug Discov Today 2020; 25: 1807–1821. https://doi.org/10.1016/j.drudis.2020.07.024

[22] WANG J, LIU Z, LI X, LI L, DOU T et al. Integrative transcriptomic and proteomics profiling analyses reveals PLK1 as a target of curcumol in hepatocellular carcinoma cells. J Funct Foods 2023; 110: 105834. https://doi.org/10.1016/j.jff.2023.105834
[23] ISLAM MR, AKASH S, RAHMAN MM, NOWRIN FT, AKTER T et al. Colon cancer and colorectal cancer: Prevention and treatment by potential natural products. Chem Biol Interact 2022; 368: 110170. https://doi.org/10.1016/j.cbi.2022.110170
[24] ZAFAR S, SARFRAZ I, RASUL A, SHAH MA, HUSSAIN G et al. Osthole: A Multifunctional Natural Compound with Potential Anticancer, Antioxidant and Anti-inflammatory Activities. Mini Rev Med Chem 2021; 21: 2747–2763. https://doi.org/10.2174/1389557520666200709175948
[25] LIU PY, CHANG DC, LO YS, HSI YT, LIN CC et al. Osthole induces human nasopharyngeal cancer cells apoptosis through Fas-Fas ligand and mitochondrial pathway. Environ Toxicol 2018; 33: 446–453. https://doi.org/10.1002/tox.22530
[26] XU X, LIU X, ZHANG Y. Osthole inhibits gastric cancer cell proliferation through regulation of PI3K/AKT. Plos One 2018; 13: e0193449. https://doi.org/10.1371/journal.pone.0193449
[27] HUANGFU M, WEI R, WANG J, QIN J, YU D et al. Osthole induces necroptosis via ROS overproduction in glioma cells. FEBS Open Bio 2021; 11: 456–467. https://doi.org/10.1002/2211-5463.13069
[28] WANG J, HUANGFU M, LI X, HAN M, LIU G et al. Osthole Induces Apoptosis and Caspase-3/GSDME-Dependent Pyroptosis via NQO1-Mediated ROS Generation in HeLa Cells. Oxid Med Cell Longev 2022; 2022: 8585598. https://doi.org/10.1155/2022/8585598
[29] WANG K, KHORAMJOO M, SRINIVASAN K, GORDON PMK, MANDAL R et al. Sequential multi-omics analysis identifies clinical phenotypes and predictive biomarkers for long COVID. Cell Rep Med 2023; 4: 101254. https://doi.org/10.1016/j.xcrm.2023.101254
[30] HE X, LIU X, ZUO F, SHI H, JING J. Artificial intelligence-based multi-omics analysis fuels cancer precision medicine. Semin Cancer Biol 2023; 88: 187–200. https://doi.org/10.1016/j.semcancer.2022.12.009
[31] ZAFARI N, BATHAEI P, VELAYATI M, KHOJASTEH-LEYLAKOOHI F, KHAZAEI M et al. Integrated analysis of multi-omics data for the discovery of biomarkers and therapeutic targets for colorectal cancer. Comput Biol Med 2023; 155: 106639. https://doi.org/10.1016/j.compbiomed.2023.106639
[32] HONG M, TAO S, ZHANG L, DIAO LT, HUANG X et al. RNA sequencing: new technologies and applications in cancer research. J Hematol Oncol 2020; 13: 166. https://doi.org/10.1186/s13045-020-01005-x
[33] MOON M, NAKAI K. Stable feature selection based on the ensemble L [1] -norm support vector machine for biomarker discovery. BMC Genomics 2016; 17: 1026. https://doi.org/10.1186/s12864-016-3320-z
[34] MASSA C, SELIGER B. Combination of multiple omics techniques for a personalized therapy or treatment selection. Front Immunol 2023; 14: 1258013. https://doi.org/10.3389/fimmu.2023.1258013
[35] YANG J, ZHU XJ, JIN MZ, CAO ZW, REN YY et al. Osthole induces cell cycle arrest and apoptosis in head and neck squamous cell carcinoma by suppressing the PI3K/AKT signaling pathway. Chem Biol Interact 2020; 316: 108934. https://doi.org/10.1016/j.cbi.2019.108934
[36] ZHU X, LI Z, LI T, LONG F, LV Y et al. Osthole inhibits the PI3K/AKT signaling pathway via activation of PTEN and induces cell cycle arrest and apoptosis in esophageal squamous cell carcinoma. Biomed Pharmacother 2018; 102: 502–509. https://doi.org/10.1016/j.biopha.2018.03.106
[37] QIU Z, OLEINICK NL, ZHANG J. ATR/CHK1 inhibitors and cancer therapy. Radiother Oncol 2018; 126: 450–464. https://doi.org/10.1016/j.radonc.2017.09.043
[38] JOO YK, BLACK EM, TRIER I, HAAKMA W, ZOU L et al. ATR promotes clearance of damaged DNA and damaged cells by rupturing micronuclei. Mol Cell 2023; 83: 3642–3658.e4. https://doi.org/10.1016/j.molcel.2023.09.003
[39] CHOU EJ, HUNG LY, TANG CJ, HSU WB, WU HY et al. Phosphorylation of CPAP by Aurora-A Maintains Spindle Pole Integrity during Mitosis. Cell Rep 2016; 14: 2975–2987. https://doi.org/10.1016/j.celrep.2016.02.085
[40] MAI Y, LIN T, ZHANG L, YANG W, LIU S et al. RAD54B inhibits vascular endothelial senescence via suppression of CHK1/p53/p21 pathway. Can J Physiol Pharmacol 2024; 102: 137–149. https://doi.org/10.1139/cjpp-2023-0192
[41] MCANDREW EN, MCMANUS KJ. The enigmatic oncogene and tumor suppressor-like properties of RAD54B: Insights into genome instability and cancer. Genes Chromosomes Cancer 2017; 56: 513–523. https://doi.org/10.1002/gcc.22458
[42] QIAO W, HUANG P, WANG X, MENG L. Susceptibility to DNA damage caused by abrogation of Rad54 homolog B: A putative mechanism for chemically induced cleft palate. Toxicology 2021; 456: 152772. https://doi.org/10.1016/j.tox.2021.152772

https://doi.org/10.4149/neo_2025_250422N178

Integrated transcriptomic and proteomic analysis reveals the mechanistic role of OST in cutaneous squamous cell carcinoma

Yue WANG[1,#], Hongfang DING[2,#], Tong GAO[1], Bocheng JI[1], Yan GAO[3], Wenjie YAN[1,*], JUANWANG[2,3,*]

Supplementary Information

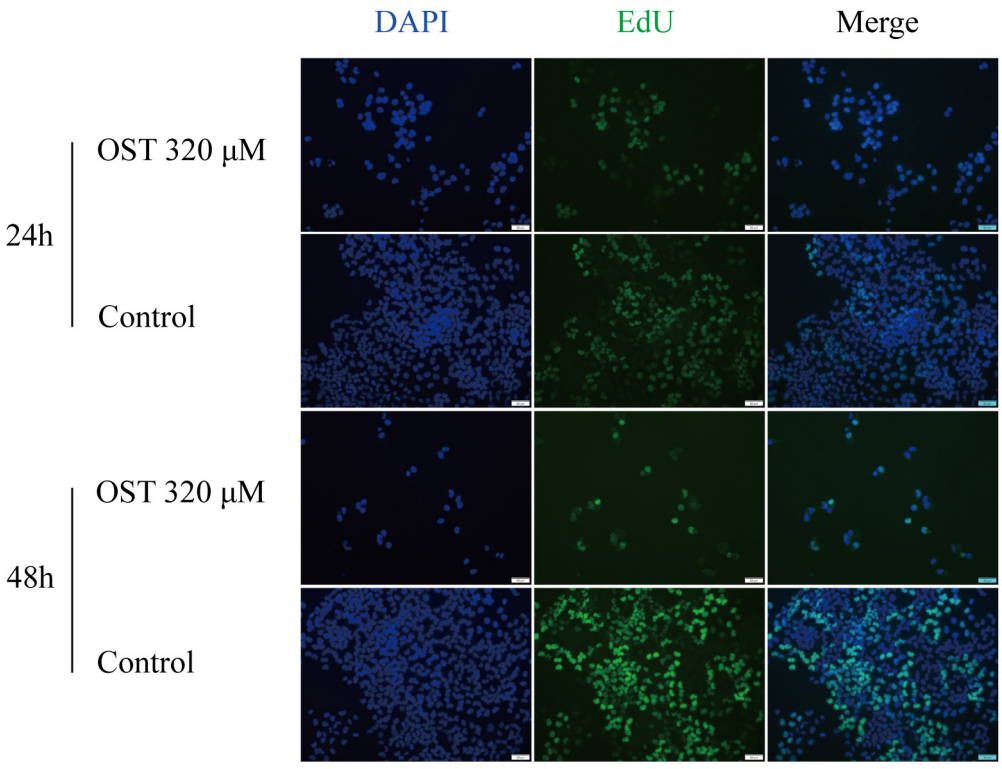

Supplementary Figure S1. OST inhibited DNA synthesis and caused S phase arrest in SCL-1 cells. SCL-1 cells were untreated or were treated with 320 μM OST for 24 h or 48 h, and then subjected to EdU staining to assess DNA synthesis (representative images shown).

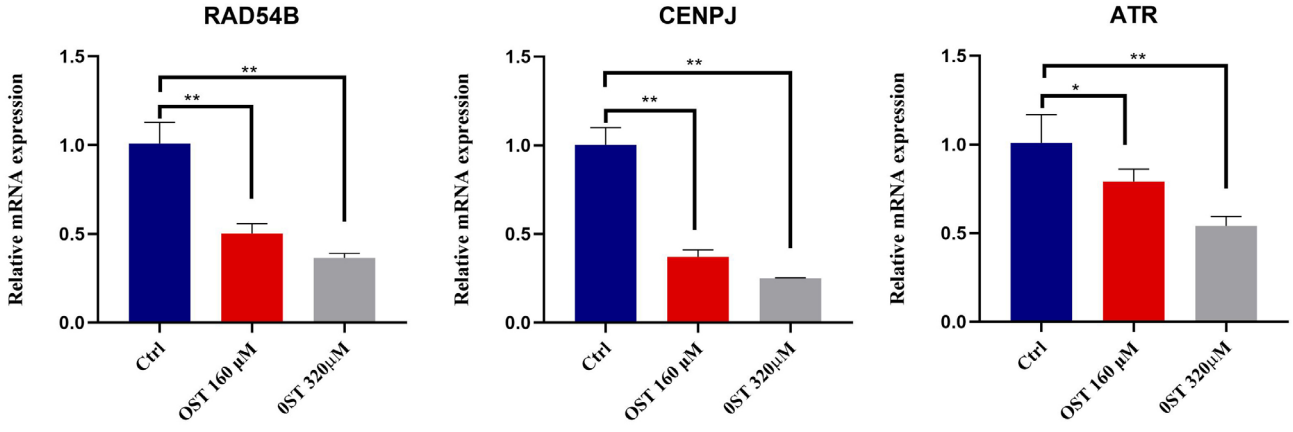

Supplementary Figure S2. OST downregulated the expression of RAD54B, CENPJ and ATR in A431 cells. The mRNA expression levels of RAD54B, CENPJ and ATR were evaluated by qPCR in A431 cells following treatment with OST (0, 160 and 320 μM). Data are expressed as the mean±SD from three independent experiments. *p<0.05, **p<0.01 compared with the control group